

Gas-phase reactivity of OH radicals with ammonia (NH₃) and methylamine (CH₃NH₂) at around 22 K

1 **Daniel González¹, Bernabé Ballesteros^{1,2}, André Canosa³, José Albaladejo^{1,2} and Elena**
2 **Jiménez^{1,2,*}**

3 ¹Departamento de Química Física, Facultad de Ciencias y Tecnologías Químicas, Universidad de
4 Castilla-La Mancha (UCLM), Avda. Camilo José Cela 1B, 13071 Ciudad Real, Spain.

5 ²Instituto de Investigación en Combustión y Contaminación Atmosférica, UCLM, Camino de
6 Moledores s/n, 13071 Ciudad Real, Spain.

7 ³ Institut de Physique de Rennes-CNRS – UMR 6251, Université de Rennes, F-35000 Rennes,
8 France.

9

10

11

12

13

14

15

16

17

18

19

20

21 *** Correspondence:**

22 Elena.Jimenez@uclm.es

23 **Keywords:** ISM, prebiotic molecules, OH radicals, CRESU technique, gas-phase reaction
24 **kinetics, ultralow temperatures**

25

26 **Abstract**

27 Interstellar molecules containing N atoms, such as ammonia (NH₃) and methylamine (CH₃NH₂),
28 could be potential precursors of amino acids like the simplest one, glycine (NH₂CH₂COOH). The
29 gas-phase reactivity of these N-bearing species with OH radicals, ubiquitous in the interstellar
30 medium, is not known at temperatures of cold dark molecular clouds. In this work, we present the
31 first kinetic study of these OH-reactions at around 22 K and different gas densities ((3.4-16.7)×10¹⁶
32 cm⁻³) in helium. The obtained rate coefficients, with ±2σ uncertainties,

33 $k_1(\text{OH}+\text{NH}_3) = (2.7\pm 0.1)\times 10^{-11} \text{ cm}^3 \text{ s}^{-1}$

34 $k_2(\text{OH}+\text{CH}_3\text{NH}_2) = (3.9\pm 0.1)\times 10^{-10} \text{ cm}^3 \text{ s}^{-1}$

35 can be included in pure gas-phase or gas-grain astrochemical models to interpret the observed
36 abundances of NH₃ and CH₃NH₂. We observed an increase of k_1 and k_2 with respect to those
37 previously measured by others at the lowest temperatures for which rate coefficients are presently
38 available: 230 K and 299 K, respectively. This increase is about 380 times for NH₃ and 20 times for
39 CH₃NH₂. Although the OH+NH₃ reaction is included in astrochemical kinetic databases, the
40 recommended temperature dependence for k_1 is based on kinetic studies at temperatures above 200
41 K. However, the OH+CH₃NH₂ reaction is not included in astrochemical networks. The observed
42 increase in k_1 at ca. 22 K **does not significantly change the abundance of NH₃ in a typical cold dark**
43 **interstellar cloud. However, the inclusion of k_2 at ca. 22 K, not considered in astrochemical**
44 **networks, indicates that the contribution of this destruction route for CH₃NH₂ is not negligible,**
45 **accounting for 1/3 of the assumed main depletion route (reaction with HCO⁺) in this IS environment.**

46

47

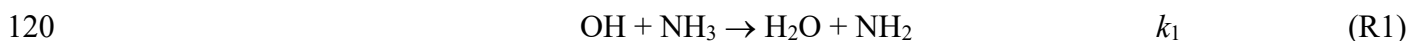
48 **Introduction**

49 Unravelling the origin of life on the Earth has been both a challenge and a matter of debate
50 for scientists throughout the history. However, what we can be certain about is that all ingredients
51 essential for life are composed by a few atoms such as H, O, C, N, or S. The combination of these
52 atoms can produce different prebiotic molecules, which are considered the precursors of life on our
53 planet. Principally, two main theories have been proposed for trying to explain how these molecules
54 could have appeared on the globe (Chyba and Sagan, 1992; Bernstein, 2006). The first one states that
55 the organic molecules that serve as the basis of life were formed in the primitive atmosphere of our
56 planet from simpler and smaller molecules (*e.g.* NH₃, CH₄, H₂O, or H₂) (Miller, 1953; Bada and
57 Lazcano, 2002; Cleaves et al., 2008). In fact, this was demonstrated experimentally by Stanley Miller
58 in the middle of the past century when he obtained a considerable number of important compounds
59 from the biological point of view, such as amino acids, from simple molecules like the
60 aforementioned, after exposing them to conditions aiming at mimicking those reigning in the
61 primitive Earth (Miller, 1953). The second one is based on the idea that the prebiotic molecules were
62 firstly synthesized in space and then, they could have been delivered to the Earth by meteorites,
63 comets, asteroids or even interplanetary dust particles (Ehrenfreund et al., 2002; Sandford et al.,
64 2020). This latter hypothesis is now in trend due to the huge and unexpected discovery in the last 70
65 years of the chemical richness in the interstellar medium (ISM). Currently, about 250 species
66 (including ions and neutrals) have been detected in the ISM or circumstellar shells (Woon, 2021).
67 Interstellar molecules, which are found in ultra-cold environments (~10-100 K), such as the so-called
68 dense or dark clouds or pre-stellar cores, range from simple diatomic molecules (*e.g.* CO or the
69 hydroxyl (OH) radical) to more complex systems (*e.g.* fullerenes). For instance, the OH radical,
70 firstly detected in Cassiopeia A in 1963 (Weinreb et al., 1963), is ubiquitous in the ISM. By
71 definition, carbon-bearing species containing 6 atoms or more are called complex organic molecules
72 (COMs) (Herbst and van Dishoeck, 2009). Some COMs containing C-O bonds (such as CH₃OH) and
73 C-N bonds (such as CH₃CN) can be potential precursors of sugars and amino acids in the presence of
74 water, respectively (Balucani, 2009), under the Earth's conditions. Although ammonia (NH₃) is not
75 considered a COM, strictly by definition, this abundant nitrogen-bearing species is very important
76 since it serves as temperature probe in molecular clouds like **Sagittarius (Sgr) B2**, where it was first
77 detected (Cheung et al., 1968). Ammonia has also been found towards a post-star forming region,
78 W3(OH), with an abundance relative to H₂ of 10⁻⁸ (Wilson et al., 1993) and in TMC-1, with a column
79 density of ~ 10¹⁵ cm⁻² (Freeman and Millar, 1983). Another interesting N-bearing species is
80 methylamine (CH₃NH₂), which was detected in the 1970s years for the first time towards Sgr B2 and
81 Orion A (Fourikis et al., 1974; Kaifu et al., 1974). Abundances relative to H₂ for CH₃NH₂ have been
82 observed to be 10⁻⁸ towards the hot core G10.47+0.33 (Ohishi et al., 2019) and 10⁻⁹ for Sgr B2
83 (Halfen et al., 2013). Both NH₃ and CH₃NH₂ have been proposed as precursors of the simplest amino
84 acid, glycine (NH₂CH₂COOH), through H-atom abstraction reactions forming NH₂ (Sorrell, 2001;
85 Garrod, 2013) and CH₂NH₂ radicals, (Woon, 2002; Garrod, 2013); however interstellar glycine
86 remains undetected in the ISM so far.

87 Under the ISM conditions, it has been assumed since a long time (Herbst and Klemperer,
88 1973) that dissociative recombination of NH₄⁺ is the main provider of NH₃ in the gas phase. This
89 cation can be generated through a series of hydrogen abstraction reactions starting from N⁺ + H₂
90 leading step by step to NH⁺, NH₂⁺, NH₃⁺ and eventually NH₄⁺ (Gerin et al., 2016; Rednyk et al.,
91 2019). Alternatively, NH₂⁺ can be produced by H₃⁺ + N (Scott et al., 1997). Although not included in
92 interstellar chemical networks, another potential source of NH₃ was recently claimed by Gianturco *et*
93 *al.* (2019) to be the reaction of the NH₂⁻ anion with H₂. Surface reactions have also been proposed as
94 plausible mechanisms to produce ammonia via a series of atomic hydrogen additions to N-hydrides

95 after NH has been formed through $N + H \rightarrow NH$ (Jonusas et al., 2020). Regarding CH_3NH_2 , different
 96 synthetic routes have been proposed. In the gas-phase, it may be formed via the radiative association
 97 between NH_3 and the methyl radical cation (CH_3^+) followed by dissociative recombination (Herbst,
 98 1985). But CH_3NH_2 can also be formed on grain surfaces by sequential hydrogenation of hydrogen
 99 cyanide (HCN), as experimentally observed by Theule *et al.* (2011). Simulations of the irradiation of
 100 CH_4 and NH_3 ices may also form CH_3NH_2 (Kim and Kaiser, 2011; Förstel et al., 2017), but also in
 101 cold and quiescent molecular clouds (Ioppolo et al., 2021). In the gas-grain chemical model by
 102 (Garrod et al., 2008), the CH_3+NH_2 reaction was also suggested as a source of CH_3NH_2 during
 103 warm-up phases.

104 It is also important to know how NH_3 and CH_3NH_2 are being destroyed to have a good insight
 105 of the chemical evolution of the ISM. Focusing on neutral-neutral reactions, reaction networks that
 106 astrochemical models used, such as KIDA and UfA, include eight depletion routes for NH_3 . *e.g.*
 107 reactions with H, CH, CN, among other radicals. Concerning CH_3NH_2 , only two depleting reactions
 108 by CH and CH_3 radicals are included in KIDA database, while UfA database does not include any.
 109 Until now, the reactivity of NH_3 with neutral radicals or atoms at ISM temperatures has been
 110 investigated experimentally in the presence of CN (Sims et al., 1994), CH (Bocherel et al., 1996),
 111 C_2H (Nizamov and Leone, 2004) and $C(^3P)$ (Bourgalais et al., 2015; Hickson et al., 2015) whereas,
 112 only the reactivity of CH_3NH_2 with CN is documented (Sleiman et al., 2018a, 2018b). Due to the
 113 important role of OH radicals as a key intermediate in multiple reactive processes in the ISM
 114 (Cazaux et al., 2010; Goicoechea et al., 2011; Acharyya et al., 2015; Linnartz et al., 2015), the kinetic
 115 database for OH-molecule reactions has been widely extended in the past years (see *e.g.* Taylor et al.,
 116 2008; Smith and Barnes, 2013; Ocaña et al., 2017, 2019; Potapov et al., 2017; Heard, 2018; Blázquez
 117 et al., 2019, 2020). For the $OH+NH_3$ reaction (Reaction R1), of interest in atmospheric and
 118 combustion chemistry, its gas-phase kinetics has been extensively studied both experimentally and
 119 theoretically.



121 Note that other reaction channels forming H_2NO+H_2 , $HNOH+H_2$, or H_2NOH+H are not
 122 thermodynamically accessible, since they are endothermic by Gibbs free energies ranging from 19.67
 123 to 31.73 kcal/mol (Vahedpour et al., 2018). Reaction R1 is also of astrochemical interest since it
 124 leads to the formation of NH_2 radicals, which were also observed towards the same location as
 125 ammonia (van Dishoeck et al., 1993). In the laboratory studies, the rate coefficient for R1, k_1 , has
 126 been reported since the 1970's by many research groups over a wide range of temperature (230-2360
 127 K) and pressures (1-4000 mbar) (Stuhl, 1973; Kurylo, 1973; Zellner and Smith, 1974; Hack et al.,
 128 1974; Perry et al., 1976; Silver and Kolb, 1980; Fujii et al., 1981, 1986; Salimian et al., 1984;
 129 Stephens, 1984; Zabielski and Seery, 1985; Jeffries and Smith, 1986; Diau et al., 1990). A summary
 130 of all previous experimental results can be found in Diau *et al.* (1990). The observed dependence of
 131 k_1 with temperature is positive, *i.e.*, the rate coefficient increases when temperature increases, and the
 132 reported activation energies range from 0.5 to 9 kcal/mol in the 230-2360 K range (Zellner and
 133 Smith, 1974; Hack et al., 1974; Perry et al., 1976; Silver and Kolb, 1980; Fujii et al., 1981, 1986;
 134 Salimian et al., 1984; Stephens, 1984; Zabielski and Seery, 1985; Jeffries and Smith, 1986; Diau et
 135 al., 1990). The computed energy barriers in the 200-4000 K range were found to be between 2.0 and
 136 9.05 kcal/mol (Giménez et al., 1992; Corchado et al., 1995; Bowdridge et al., 1996; Nyman, 1996;
 137 Lynch et al., 2000; Monge-Palacios et al., 2013b; Nguyen and Stanton, 2017). The reaction
 138 mechanism of R1 was also theoretically investigated (Giménez et al., 1992; Espinosa-García and
 139 Corchado, 1994; Corchado et al., 1995; Bowdridge et al., 1996; Nyman, 1996; Lynch et al., 2000;
 140 Monge-Palacios et al., 2013b; Nguyen and Stanton, 2017). The formation of a pre-reactive complex

141 (PRC) at the entrance channel is accepted, as illustrated in Scheme 1, and quantum mechanical
 142 tunneling has been reported to be an important contribution to k_1 , leading to the observed non-
 143 Arrhenius behavior (Espinosa-García and Corchado, 1994; Corchado et al., 1995; Bowdridge et al.,
 144 1996; Nyman, 1996; Monge-Palacios et al., 2013b; Nguyen and Stanton, 2017).

145 Regarding the OH+CH₃NH₂ reaction (Reaction R2), previous kinetic studies are restricted to
 146 temperatures higher than 295 K (Atkinson et al., 1977; Carl and Crowley, 1998; Onel et al., 2013;
 147 Butkovskaya and Setser, 2016). From the experimental point of view, Atkinson *et al.* (1977) and
 148 Onel *et al.* (2013) reported the temperature dependence of reaction R2 in the 299-426 K and 298-600
 149 K ranges, respectively. A negative temperature dependence of k_2 was observed and this rate
 150 coefficient increases when temperature decreases.



152 Reaction R2 may proceed by H-abstraction from methyl (-CH₃) or amino (-NH₂) groups forming
 153 CH₂NH₂ and CH₃NH radicals plus water, respectively. The formation of CH₂NH₂ radicals was
 154 measured to be the main reaction channel at room temperature (Nielsen et al., 2011, 2012; Onel et al.,
 155 2014; Butkovskaya and Setser, 2016), in agreement with theoretical predictions at 299 K and above
 156 (Galano and Alvarez-Idaboy, 2008; Tian et al., 2009). These calculations suggest a stepwise
 157 mechanism involving the formation of a PRC at the entrance channels and an energy barrier of a few
 158 kcal/mol for the H-abstraction channel from -CH₃ group, as depicted in Scheme 2.

159 As there are no kinetic data of k_1 and k_2 at temperatures of the cold dark interstellar clouds and
 160 since they are necessary to properly model the chemistry of the ISM, we present in this work the first
 161 determination of the rate coefficient for the reactions of NH₃ and CH₃NH₂, k_i ($i=1$ or 2), with OH
 162 radicals at ca. 22 K using a combination of a pulsed CRESU (French acronym for *Reaction Kinetics*
 163 *in a Uniform Supersonic Flow*) reactor with laser techniques. The implications of the reported new
 164 rate coefficients will be discussed in terms of their effect on the predicted abundances of NH₃ and
 165 CH₃NH₂ in a typical cold dark interstellar cloud at 10 K.

166

167 Experimental methods

168 *CRESU apparatus coupled to pulsed laser photolysis-laser induced fluorescence technique*

169 The experimental system based on the pulsed uniform supersonic expansion of a gas mixture has
 170 been already described elsewhere (Jiménez et al., 2015, 2016; Antiñolo et al., 2016; Canosa et al.,
 171 2016; Ocaña et al., 2017, 2018, 2019; Blázquez et al., 2019, 2020; Neeman et al., 2021). To carry out
 172 the kinetic experiments, three Laval nozzles (He23-HP, He23-IP, and He23-LP) were used with
 173 helium as a carrier gas. These nozzles were designed to generate a uniform flow at around 22 K for
 174 three different jet pressures (see Table 1) (Jiménez et al., 2015; Canosa et al., 2016; Ocaña et al.,
 175 2017), thus allowing us to explore the influence of pressure on the reactivity at a constant
 176 temperature. Bath gas and reactants (NH₃ or CH₃NH₂) were introduced in the CRESU chamber
 177 through calibrated mass flow controllers, MFCs (Sierra Instruments, Inc., model Smart Trak, Smart-
 178 Trak 2, MicroTrak 101 and Smart-Trak 100). CH₃NH₂ was diluted in He and stored in a 20-L or 50-L
 179 bulb. Calibrated mass flow rates of these diluted mixtures ranged from 6.6 to 200 sccm (standard
 180 cubic centimeters per minute), depending on the Laval nozzle used. Dilution factor f ranged from
 181 1.78×10^{-2} to 4.54×10^{-2} . In contrast, NH₃ was flown directly to the pre-expansion chamber (*reservoir*)
 182 from a gas cylinder through a MFC manufactured with anticorrosive materials (Sierra Instruments,
 183 Inc., model Smart-Trak 100). The flow rates of pure NH₃ ranged from 3 to 15 sccm. The OH-

184 precursor employed was H₂O₂, since it is a clean source of OH radicals. Gaseous H₂O₂ was
 185 introduced into the *reservoir* by bubbling the bath gas through an aqueous solution of H₂O₂, as
 186 explained in Jiménez *et al.* (2005). The flow rate of He through the H₂O₂ bubbler in different
 187 experiments ranged from 35.6 to 265.8 sccm, depending on the Laval nozzle used. Within a kinetic
 188 experiment, this flow rate was kept constant to maintain invariable the contribution of the OH loss
 189 due to the OH+H₂O₂ reaction (see kinetic analysis). The gas mixture formed by He (main flow),
 190 He/H₂O₂, and the reactant was pulsed by a two holes rotary disk described in Jiménez *et al.* (2015).

191 After the gas expansion through the Laval nozzle, the jet temperature was measured by a Pitot
 192 tube to be (21.7±1.4) K for the He23-HP nozzle, (22.5±0.7) K for the He23-IP nozzle, and (21.1±0.6)
 193 K for the He-23LP nozzle, respectively. Within the fluctuation along the flow axis (±σ), the jet
 194 temperature in all cases is ca. 22 K. The procedure to determine the jet temperature and gas density
 195 has been previously described (Jiménez *et al.*, 2015; Canosa *et al.*, 2016; Ocaña *et al.*, 2017). Pulsed
 196 photolysis of H₂O₂(g) at 248 nm was achieved by the radiation coming from a KrF excimer laser
 197 (Coherent, model ExciStar XS 200) with energies at the exit of the nozzle ranging from 0.5 to 0.9
 198 mJ/pulse at 10 Hz, depending on the nozzle used. OH radicals were monitored by collecting the laser
 199 induced fluorescence (LIF) at 310 nm, after laser excitation at *ca.* 282 nm, as a function of the
 200 reaction time defined as the time delay between the probe laser pulse and the excimer one.

201

202 *Kinetic analysis*

203 In Fig. 1 an example of the temporal evolution of the LIF intensity (I_{LIF}) is presented. As explained in
 204 several papers (Jiménez *et al.*, 2015; Ocaña *et al.*, 2018), the observed rise of the I_{LIF} signal at $t>0$ is
 205 due to rotational relaxation of OH, **coming from H₂O₂ photodissociation**, that occurs in a timescale
 206 (t_0) of less than 30 μs under the conditions of the experiments, especially, at the concentration levels
 207 of the reactant, which is an effective quencher. The fit of the recorded I_{LIF} profiles to an exponential
 208 decay (solid lines in Fig. 1) confirms that the OH loss follows a pseudo-first order kinetics.

$$209 \quad I_{LIF}(t) = I_{LIF}(t_0) \exp^{-k'(t-t_0)} \quad (\text{E1})$$

210 The pseudo-first order rate coefficient, k' , includes all the OH loss processes occurring
 211 simultaneously in the cold jet.

$$212 \quad k' = k'_0 + k_i[\text{Reactant}] \quad (\text{E2})$$

213 where k_i ($i=1$ or 2) is the bimolecular rate coefficients for OH-reactions with NH₃ (R1) and CH₃NH₂
 214 (R2). In the absence of reactant, k'_0 was measured, and it included the loss of OH radicals by OH-
 215 reaction with H₂O₂ and other OH losses, such as diffusion out of the detection zone. In Table 1, the
 216 ranges of the employed reactant concentration, [Reactant], and the determined $k'-k'_0$ values are
 217 summarized. According to Eq. (E2), the slopes of the $k'-k'_0$ *versus* [Reactant] plots yield the
 218 bimolecular rate coefficients k_i . Nevertheless, the linear relationship between $k'-k'_0$ and [Reactant] is
 219 not always accomplished, as shown in the example in Figure 2. In this figure, a downward curvature
 220 in the plot of $k'-k'_0$ *versus* [CH₃NH₂] was observed at concentrations higher than 3×10^{13} cm⁻³. As
 221 discussed in previous works (Ocaña *et al.*, 2017, 2019; Blázquez *et al.*, 2020; Neeman *et al.*, 2021),
 222 this curvature may be the result of the dimerization of the OH-co reactant, CH₃NH₂ in this case.
 223 **Considering the onset of dimerization**, the red straight line in Fig. 2 represents the fit to Eq. (E2) **at**
 224 **[CH₃NH₂] below $\sim 3 \times 10^{13}$ cm⁻³**. In contrast, for reaction R1 the plot of $k'-k'_0$ *versus* [NH₃] is linear

225 over the entire concentration range, as displayed in Fig. 3.a. Since this concentration range is much
 226 larger than the one for CH₃NH₂ and that the reactivity with OH is significantly slower for NH₃ than
 227 for CH₃NH₂, it shows that the dimerization of NH₃ is much less efficient than that of CH₃NH₂ at 22
 228 K. In Figure 3.b., all kinetic data obtained in the linear part of the $k'-k'_0$ versus [CH₃NH₂] plot are
 229 depicted. The bimolecular rate coefficient k_2 at ca. 22 K is, then, obtained from the slope of such a
 230 plot.

231

232 *Reagents.* Gases: He (99.999%, Nippon gases), NH₃ (≥99.95%, Merck) and CH₃NH₂ (≥99.0%,
 233 Merck) were used as supplied. Aqueous solution of H₂O₂ (Sharlab, initially at 50% w/w) was pre-
 234 concentrated as explained earlier (Albaladejo et al., 2003).

235

236 Results and discussion

237 The OH+NH₃ reaction

238 *Temperature dependence of k_1*

239 A summary of the individual rate coefficients k_1 obtained at 22 K and different total pressures of the
 240 gas jet is presented in Table 1. Within the stated statistical uncertainties ($\pm 2\sigma$), no pressure
 241 dependence of k_1 was observed in the investigated range (0.10-0.51 mbar). For this reason, we
 242 combined all the kinetic results, as shown in Fig. 3.a. The resulting rate coefficient for the OH+NH₃
 243 reaction at ca. 22 K is:

$$244 \quad k_1(\sim 22 \text{ K}) = (2.7 \pm 0.1) \times 10^{-11} \text{ cm}^3 \text{ s}^{-1}$$

245 where the uncertainty ($\pm 2\sigma$) only includes statistical errors. An additional 10% uncertainty has to be
 246 added to account for the systematic errors.

247 As mentioned in the Introduction section, reaction R1 has been investigated under extensive
 248 experimental conditions of temperature (230-2360) K and pressure (1-4000 mbar). A summary of all
 249 previous kinetic studies can be found in the most recent investigation from Diau *et al.* (1990).
 250 Focusing on the works carried out as a function of temperature (Zellner and Smith, 1974; Hack et al.,
 251 1974; Perry et al., 1976; Silver and Kolb, 1980; Fujii et al., 1981, 1986; Salimian et al., 1984;
 252 Stephens, 1984; Zabielski and Seery, 1985; Jeffries and Smith, 1986; Diau et al., 1990), a positive
 253 temperature dependence of k_1 was observed in all cases, as shown in Figure 4.a. For instance, IUPAC
 254 recommends a T-expression for k_1 , based on previous results below 450 K (Zellner and Smith, 1974;
 255 Perry et al., 1976; Silver and Kolb, 1980; Stephens, 1984; Diau et al., 1990), with an E_a/R factor of
 256 925 K which yields an activation energy (E_a) of 1.8 kcal/mol (Atkinson et al., 2004):

$$257 \quad k_1(230 - 450 \text{ K}) = 3.5 \times 10^{-12} \exp^{-925 \text{ K}/T} \text{ cm}^3 \text{ s}^{-1} \quad (\text{E3})$$

258 Even so, as hydrogen atom transfer reactions usually show significant dynamical quantum effects
 259 (see Reaction mechanism), the kinetics of reaction R1 deviates from the Arrhenius behavior, showing
 260 a curvature in the plot of $\ln k_1$ versus $1/T$. This deviation from Arrhenius behavior has been observed
 261 experimentally between 840 and 1425 K (Jeffries and Smith, 1986) and predicted theoretically

262 between 5 and 4000 K (Espinosa-García and Corchado, 1994; Corchado et al., 1995; Monge-Palacios
 263 et al., 2013b; Nguyen and Stanton, 2017; Vahedpour et al., 2018). Most of the computed k_1 have
 264 been reported at temperatures higher than 200 K (Espinosa-García and Corchado, 1994; Corchado et
 265 al., 1995; Monge-Palacios et al., 2013b; Vahedpour et al., 2018). Only the calculations by Nguyen
 266 and Stanton (2017) were performed at lower temperatures and down to 5 K. For ease of presentation,
 267 kinetic data between 170 K and 4000 K are plotted in Fig. 4.b in Arrhenius form to clearly show the
 268 curvature. Down to 20 K, the predicted k_1 by Nguyen and Stanton (2017), represented by a pink line
 269 in Figure 4.c, was $2 \times 10^{-16} \text{ cm}^3 \text{ s}^{-1}$. This value is around 5 orders of magnitude lower than the
 270 experimental result reported in this work. Certainly, further kinetic studies between 230 K and 22 K
 271 (and even below) are needed and are planned in our laboratory in the future.

272 *Reaction mechanism*

273 As stated in the Introduction section, the reaction mechanism of the OH+NH₃ reaction has been
 274 widely studied from a theoretical point of view. The effects of vibrational and translational energy of
 275 NH₃ and OH counter partners have been studied by quasi-classical trajectories (Nyman, 1996;
 276 Monge-Palacios and Espinosa-Garcia, 2013; Monge-Palacios et al., 2013a) and by quantum
 277 scattering calculations (Nyman, 1996). Besides these dynamical studies, *ab initio* calculations based
 278 on the transition state theory (TST) were reported. In scheme 1, a simplified illustration of the
 279 relative energies to the reactants of the stationary points along the minimum energy pathway (MEP)
 280 for the OH+NH₃ system is shown. Some studies proposed that product formation in reaction R1
 281 occurs from the transition state and reported energy barriers ranged from 2.03 kcal/mol to 8.94
 282 kcal/mol (Giménez et al., 1992; Bowdridge et al., 1996; Lynch et al., 2000). However, other
 283 investigations proposed that reaction R1 occurs through a H-bonded PRC at the entrance channel
 284 (Corchado et al., 1995; Bowdridge et al., 1996; Monge-Palacios et al., 2013b; Nguyen and Stanton,
 285 2017). The relative energy of this PRC is positioned a few kcal/mol above the reactants (Nguyen and
 286 Stanton, 2017) or -1.8 kcal/mol (Corchado et al., 1995; Monge-Palacios et al., 2013b). In addition to
 287 the PRC, a H-bonded complex near the products (PPC, pre-product complex) (Espinosa-García and
 288 Corchado, 1994; Corchado et al., 1995; Monge-Palacios et al., 2013b; Nguyen and Stanton, 2017) is
 289 proposed at the exit channel, which is stabilized with respect to the reactants by *ca.* -15 kcal/mol.
 290 Table 2 summarizes the relative energies of PRC, TS, and PPC from theoretical calculations reported
 291 in the literature.

292 Note that the reaction pathway for the OH+NH₃ system is qualitatively similar to the one calculated
 293 for the OH+CH₃OH reaction (Ocaña et al., 2019), *i.e.* formation of a H-bonded PRC followed by a
 294 transition state with a positive energy barrier. Following that comparison, the observed increase of k_1
 295 can be interpreted by the formation of a long-lived PRC at very low temperatures, which surpasses
 296 the energy barrier by quantum mechanical tunnelling.

297 *Effect of k_1 in the abundance of interstellar NH₃*

298 Astrochemical networks apply modified Arrhenius expressions to estimate rate coefficients in a
 299 certain temperature interval:

$$300 \quad k(T) = \alpha \left(\frac{T}{300\text{K}} \right)^\beta \exp^{-\gamma/T} \quad (\text{E4})$$

301 For example, KIDA database uses the recommended expression by Atkinson *et al.* (2004)
 302 (expression E3, where $\beta=0$) and UDfA database uses the following expression:

$$303 \quad k_1(200 - 3000 \text{ K}) = 1.47 \times 10^{-13} \left(\frac{T}{300\text{K}} \right)^{2.05} \exp^{-7 \text{ K}/T} \text{ cm}^3 \text{ s}^{-1} \quad (\text{E5})$$

304 Note that these recommended expressions (E3) and (E5) are valid on the stated temperature range.
 305 Using these T-expressions to extrapolate rate coefficients down to 22 K is extremely risky. One gets
 306 very low values of k_1 , on the order of $10^{-27} \text{ cm}^3 \text{ s}^{-1}$ from KIDA expression (E3) and $10^{-16} \text{ cm}^3 \text{ s}^{-1}$ from
 307 UDfA (E5), compared with the rate coefficient for the OH+NH₃ reaction determined in the present
 308 work. Using Eqs. (E3) and (E5), the rate coefficient at 230 K, $k_1(230 \text{ K})$, and extrapolated $k_1(200 \text{ K})$
 309 are 6.4 and $8.3 \times 10^{-14} \text{ cm}^3 \text{ s}^{-1}$, respectively. At the lowest temperature, the $k_1(\sim 22 \text{ K})/k_1(230 \text{ K})$ ratio is
 310 around 380. This value means that the rate of formation of NH₂ radicals from the reaction of NH₃
 311 with OH radicals is really enhanced by more than two orders of magnitude at the typical temperature
 312 of a cold dark cloud. Using k_1 , obtained in this work, and the rate coefficients from the KIDA and
 313 UDfA databases, for a typical cold dark cloud, with H₂ molecular density of $1 \times 10^4 \text{ cm}^{-3}$ and a
 314 temperature of 10 K (close to the one reproduced in this work) (Agúndez and Wakelam, 2013), the
 315 change in modelled abundances of NH₃ is negligible for both reaction networks. The main
 316 destruction route for NH₃ in this cold environment is the reaction with H₃O⁺ cations, being the
 317 reaction of NH₃ with OH radicals around 1% of that with H₃O⁺ species.

318

319 The OH+CH₃NH₂ reaction

320 *Temperature dependence of k_2*

321 As shown in Table 1, no pressure dependence of the rate coefficient for the OH+CH₃NH₂ reaction
 322 was observed in the investigated range. The resulting k_2 at ca. 22 K from the combination of all
 323 kinetic data at different gas densities (see Fig. 3.b) is:

$$324 \quad k_2(\sim 22 \text{ K}) = (3.9 \pm 0.1) \times 10^{-10} \text{ cm}^3 \text{ s}^{-1}$$

325 This value together with previously reported k_2 over the 298-3000 K temperature range (Atkinson *et*
 326 *al.*, 1977; Carl and Crowley, 1998; Tian *et al.*, 2009; Onel *et al.*, 2013; Butkovskaya and Setser,
 327 2016) are depicted in Figure 5. The temperature dependence of k_2 was first measured by Atkinson *et*
 328 *al.* (1977) at T>299 K, who reported the following Arrhenius expression:

$$329 \quad k_2(299 - 426 \text{ K}) = 1.02 \times 10^{-11} \exp^{(455 \pm 300) \text{ cal mol}^{-1}/RT} \text{ cm}^3 \text{ s}^{-1} \quad (\text{E6})$$

330 The activation energy is slightly negative in this case, -0.45 kcal/mol; however more recently, the
 331 negative temperature dependence observed experimentally for reaction R2 was also reported by Onel
 332 *et al.* (2013) as an expression with no activation energy and a T-dependent pre-exponential factor
 333 (black circles in Fig. 5):

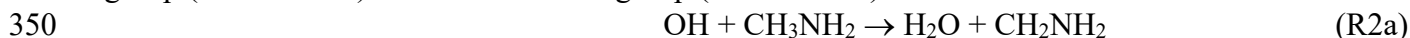
$$334 \quad k_2(298 - 500 \text{ K}) = 1.89 \times 10^{-11} \left(\frac{T}{298\text{K}} \right)^{-0.56} \text{ cm}^3 \text{ s}^{-1} \quad (\text{E7})$$

335 Using the experimental Onel's expression, the extrapolated $k_2(\sim 22 \text{ K})$ is ca. $8 \times 10^{-11} \text{ cm}^3 \text{ s}^{-1}$ (4.9 times
 336 lower than the experimental one reported here), while expression (E6) provides an extrapolated
 337 $k_2(\sim 22 \text{ K})$ of $3.4 \times 10^{-7} \text{ cm}^3 \text{ s}^{-1}$, which is a non-realistic value for a neutral-neutral reaction. Onel *et al.*
 338 (2013) also computed k_2 between 200 and 500 K (blue line in Fig. 5) to be around 60% higher than
 339 the experimental values. No experimental kinetic data have been reported at T>500 K, however Tian
 340 *et al.* (2009) predicted a minimum of k_2 around 550 K and a remarkable increase of k_2 at higher

341 temperatures, *i.e.*, the rate coefficient for the OH+CH₃NH₂ reaction is expected to exhibit a non-
 342 Arrhenius behavior. As shown by dashed lines in Fig. 5, the extrapolated k_2 from calculations of Onel
 343 *et al.* (2013) is in excellent agreement with our reported value and the value of k_2 obtained by
 344 extrapolation of Tian *et al.* (2009) data is only a factor of ca. 2 lower than the experimental value
 345 reported in this work. Additional kinetic studies between 298 K and 22 K are clearly needed to
 346 confirm the expected trend in the T-dependence of k_2 .

347 *Reaction mechanism*

348 The possible exothermic reaction channels for reaction R2 are the H-abstraction from the methyl
 349 group (channel R2a) or from the amino group (channel R2b):



352 Theoretically, the mechanism of reaction R2 has been investigated by several groups (Galano and
 353 Alvarez-Idaboy, 2008; Tian *et al.*, 2009; Onel *et al.*, 2013; Borduas *et al.*, 2016). The calculations
 354 suggest a stepwise mechanism involving the formation of a PRC in the entrance channels (Tian *et al.*,
 355 2009; Onel *et al.*, 2013; Borduas *et al.*, 2016) and a PPC in the exit channels (Tian *et al.*, 2009; Onel
 356 *et al.*, 2013). On the other hand, the OH-addition to N and subsequent concerted C-C cleavage, which
 357 produces CH₃ radicals and NH₂OH, is endothermic with an energy barrier of 37.4 kcal/mol (Borduas
 358 *et al.*, 2016). For that reason, in scheme 2, the energies of the stationary points along the MEP for the
 359 OH+CH₃NH₂ reaction is only depicted for the exothermic channels R2a and R2b. In the 299–3000 K
 360 temperature range, the dominant exothermic channel is that producing CH₂NH₂ radicals (Galano and
 361 Alvarez-Idaboy, 2008; Tian *et al.*, 2009). The branching ratio for R2a (r) at 298 K was reported to be
 362 of 0.797 (Galano and Alvarez-Idaboy, 2008) and 0.74 (Tian *et al.*, 2009). In contrast, Borduas *et al.*
 363 (2016) concluded that channels R2a and R2b are competitive, with energy barriers close to the
 364 entrance level energies of the reactants and within 1 kcal mol⁻¹ of each other. Nevertheless, the
 365 dominance of R2a channel at room temperature has experimentally been confirmed by Nielsen *et al.*
 366 (2011, 2012), Onel *et al.* (2014), and Butkovskaya and Setser (2016). Nielsen *et al.* (2011, 2012)
 367 performed experiments in EUPHORE atmospheric chamber providing a r of (0.75 ± 0.05) for
 368 channel R2a. A similar value (0.79 ± 0.15) was found by Onel *et al.* (2014) and by Butkovskaya and
 369 Setser (2016) (0.74 ± 0.05) No measurements or calculations were found at temperatures below room
 370 temperature. Thus, further theoretical and/or experimental studies are needed to know what the
 371 branching ratios of channels R2a (forming CH₂NH₂) and R2b (forming CH₃NH) are at interstellar
 372 temperatures.

374 *Effect of k_2 in the abundance of interstellar CH₃NH₂*

375 Neither KIDA database nor UDFa network include this OH-reaction as a potential destruction route
 376 for CH₃NH₂. However, this reaction is extremely fast at ca. 22 K as it is shown by the experimental
 377 rate coefficient for the OH+CH₃NH₂ reaction reported here. Our measured k_2 (~22 K) would, then,
 378 lead to a quicker depletion of CH₃NH₂ by reaction with OH in astrochemical models. The k_2 (~22
 379 K)/ k_2 (298 K) ratio is around 20, indicating that the use of k_2 (298 K) in modelling the ISM would
 380 underestimate the loss of CH₃NH₂ by OH by more than one order of magnitude. Using the reported
 381 k_2 (~22 K) in the pure gas-phase model from Agúndez and Wakelam (2013), the destruction of
 382 CH₃NH₂ by OH radicals in a typical cold dark cloud (H₂ molecular density of 1×10⁴ cm⁻³ and
 383 temperature 10 K) supposes around 1/3 of that initiated by HCO⁺ (main depletion route).

384
 385

386 Conclusions

387 The OH-reactivity of NH₃ at ca. 22 K is more than two orders of magnitude higher than that observed
388 at the lowest temperature achieved up to now, 230 K. This confirms that the observed curvature in
389 the Arrhenius plot reflects the increase of k_1 at low temperatures. Further studies are needed to
390 complete the kinetic behavior between 22 K and 230 K and lower temperatures than 22 K. For
391 CH₃NH₂, the determined rate coefficient at ca. 22 K is almost 20 times higher than the one measured
392 at room temperature. The slightly negative temperature dependence of k_2 observed by Atkinson *et al.*
393 (1977) at T > 298 K, implies that the OH-reactivity increases at temperatures lower than room
394 temperature, as observed in this work. These new experimental data indicate that the inclusion of the
395 rate coefficient for the OH+NH₃ reaction at 20 K in gas-phase astrochemical models does not
396 significantly change the abundance of NH₃ in a typical cold dark cloud since the main destruction
397 route for NH₃ is the reaction with H₃O⁺. However, the inclusion of the rate coefficient for the
398 OH+CH₃NH₂ reaction at 20 K, not considered in KIDA and UDfA networks, indicated that the
399 contribution of this destruction route is not negligible, accounting for 1/3 of the main assumed
400 depletion route (reaction with HCO⁺) in this IS environment with temperature close to 10 K.
401

402 Conflict of Interest

403 *The authors declare that the research was conducted in the absence of any commercial or financial*
404 *relationships that could be construed as a potential conflict of interest.*

405 Author Contributions

406 D.G. performed the experiments, analyzed the kinetic data, and wrote the draft of the article; B.B.
407 and E.J. contributed to the design and supervision of the experiments; A.C. and E.J. participated in
408 the critical revision of the article; J.A. and E.J. got the funds for carrying out this research and
409 managed the projects. All authors discussed the results and contributed to the final manuscript.

410 Funding

411 This work has been supported by the Spanish Ministry of Science and Innovation (MICINN) through
412 the CHEMLIFE project (Ref.: PID2020-113936GB-I00), the regional government of Castilla-La
413 Mancha through CINEMOL project (Ref.: SBPLY/19/180501/000052) and by the University of
414 Castilla-La Mancha – UCLM (*Ayudas para la financiación de actividades de investigación dirigidas*
415 *a grupos* (REF: 2019-GRIN-27175). D. González also acknowledges UCLM (*Plan Propio de*
416 *Investigación*) for funding his contract during the performance of this investigation.

417

418 Acknowledgments

419 The authors acknowledge Francisco J. Maigler for his technical assistance during the performance of
420 these experiments and Dr. Marcelino Agúndez for helpful discussion on the effect of current rate
421 coefficients on the abundance of NH₃ and CH₃NH₂ in a typical cold dark cloud.

422

423

424 **References**

- 425 Acharyya, K., Herbst, E., Caravan, R. L., Shannon, R. J., Blitz, M. A., and Heard, D. E. (2015).
426 Molecular Physics : An International Journal at the Interface Between Chemistry and Physics
427 The importance of OH radical – neutral low temperature tunnelling reactions in interstellar
428 clouds using a new model. *Astron. Astrophys* 113, 2243–2254.
- 429 Agúndez, M., and Wakelam, V. (2013). Chemistry of Dark Clouds: Databases, Networks, and
430 Models. *Chem. Rev.* 113, 8710–8737. doi:10.1021/cr4001176.
- 431 Albaladejo, J., Ballesteros, B., Jiménez, E., Díaz de Mera, Y., and Martínez, E. (2003). Gas-phase
432 OH radical-initiated oxidation of the 3-halopropenes studied by PLP-LIF in the temperature
433 range 228–388 K. *Atmos. Environ.* 37, 2919–2926. doi:10.1016/S1352-2310(03)00297-8.
- 434 Antiñolo, M., Agúndez, M., Jimenez, E., Ballesteros, B., Canosa, A., Dib, G. El, et al. (2016).
435 Reactivity of OH and CH₃OH between 22 and 64 K: Modelling the gas phase production of
436 CH₃O in Barnard 1b. *Astrophys. J.* 823, 25. doi:10.3847/0004-637X/823/1/25.
- 437 Atkinson, R., Baulch, D. L., Cox, R. A., Crowley, J. N., Hampson, R. F., Hynes, R. G., et al. (2004).
438 Evaluated kinetic and photochemical data for atmospheric chemistry: Part 1 – gas phase
439 reactions of O_x, HO_x, NO_x and SO_x species. *Atmos. Chem. Phys.* 4, 1461–1738.
440 doi:10.5194/acpd-3-6179-2003.
- 441 Atkinson, R., Perry, R. A., and Pitts, J. N. (1977). Rate constants for the reaction of the OH radical
442 with CH₃SH and CH₃NH₂ over the temperature range 299–426°K. *J. Chem. Phys.* 66, 1578–
443 1581. doi:10.1063/1.434076.
- 444 Bada, J. L., and Lazcano, A. (2002). Some like it hot, but not the first biomolecules. *Science* (80-.).
445 296, 1982–1983. doi:10.1126/science.1069487.
- 446 Balucani, N. (2009). Elementary reactions and their role in gas-phase prebiotic chemistry. *Int. J. Mol.*
447 *Sci.* 10, 2304–2335. doi:10.3390/ijms10052304.
- 448 Bernstein, M. (2006). Prebiotic materials from on and off the early Earth. *Philos. Trans. R. Soc. B*
449 *Biol. Sci.* 361, 1689–1702. doi:10.1098/rstb.2006.1913.
- 450 Blázquez, S., González, D., García-Sáez, A., Antiñolo, M., Bergeat, A., Caralp, F., et al. (2019).
451 Experimental and Theoretical Investigation on the OH+CH₃C(O)CH₃. Reaction at Interstellar
452 Temperatures (T=11.7–64.4 K). *ACS Earth Sp. Chem.* 3, 1873–1883.
453 doi:10.1021/acsearthspacechem.9b00144.
- 454 Blázquez, S., González, D., Neeman, E. M., Ballesteros, B., Agúndez, M., Canosa, A., et al. (2020).
455 Gas-phase kinetics of CH₃CHO with OH radicals between 11.7 and 177.5 K. *Phys. Chem.*
456 *Chem. Phys.* 22, 20562–20572. doi:10.1039/D0CP03203D.
- 457 Bocherel, P., Herbert, L. B., Rowe, B. R., Sims, I. R., Smith, I. W. M., and Travers, D. (1996).
458 Ultralow-Temperature Kinetics of CH(X²Π) Reactions: Rate Coefficients for Reactions with O₂
459 and NO (T = 13–708 K), and with NH₃ (T = 23–295 K). *J. Phys. Chem.* 100, 3063–3069.
460 doi:10.1021/jp952628f.

- 461 Borduas, N., Abbatt, J. P. D., Murphy, J. G., So, S., and Da Silva, G. (2016). Gas-Phase Mechanisms
 462 of the Reactions of Reduced Organic Nitrogen Compounds with OH Radicals. *Environ. Sci.*
 463 *Technol.* 50, 11723–11734. doi:10.1021/acs.est.6b03797.
- 464 Bourgalais, J., Capron, M., Kailasanathan, R. K. A., Osborn, D. L., Hickson, K. M., Loison, J. C., et
 465 al. (2015). The C(³P) + NH₃ reaction in interstellar chemistry: I. Investigation of the product
 466 formation channels. *Astrophys. J.* 812, 1–40. doi:10.1088/0004-637X/812/2/106.
- 467 Bowdridge, M., Furue, H., and Pacey, P. D. (1996). Properties of transition species in the reactions of
 468 hydroxyl with ammonia and with itself. *J. Phys. Chem.* 100, 1676–1681.
 469 doi:10.1021/jp9522573.
- 470 Butkovskaya, N. I., and Setser, D. W. (2016). Branching Ratios and Vibrational Distributions in
 471 Water-Forming Reactions of OH and OD Radicals with Methylamines. *J. Phys. Chem. A* 120,
 472 6698–6711. doi:10.1021/acs.jpca.6b06411.
- 473 Canosa, A., Ocaña, A. J., Antiñolo, M., Ballesteros, B., Jiménez, E., and Albaladejo, J. (2016).
 474 Design and testing of temperature tunable de Laval nozzles for applications in gas-phase
 475 reaction kinetics. *Exp. Fluids* 57. doi:10.1007/s00348-016-2238-1.
- 476 Carl, S. A., and Crowley, J. N. (1998). Sequential Two (Blue) Photon Absorption by NO₂ in the
 477 Presence of H₂ as a Source of OH in Pulsed Photolysis Kinetic Studies: Rate Constants for
 478 Reaction of OH with CH₃NH₂, (CH₃)₂NH, (CH₃)₃N, and C₂H₅NH₂ at K. *J. Phys. Chem. A* 102,
 479 8131–8141. doi:10.1021/jp9821937.
- 480 Cazaux, S., Cobut, V., Marseille, M., Spaans, M., and Caselli, P. (2010). Water formation on bare
 481 grains: When the chemistry on dust impacts interstellar gas. *Astron. Astrophys.* 522, A74.
 482 doi:10.1051/0004-6361/201014026.
- 483 Cheung, A. C., Rank, D. M., Townes, C. H., Thornton, D. D., and Welch, W. J. (1968). Detection of
 484 NH₃ Molecules in the Interstellar Medium by Their Microwave Emission. *Phys. Rev. Lett.* 21,
 485 1701–1705. doi:10.1103/PhysRevLett.21.1701.
- 486 Chyba, C., and Sagan, C. (1992). Endogenous production, exogenous delivery and impact-shock
 487 synthesis of organic molecules: an inventory for the origins of life. *Nature* 355, 125–132.
 488 doi:10.1038/355125a0.
- 489 Cleaves, H. J., Chalmers, J. H., Lazcano, A., Miller, S. L., and Bada, J. L. (2008). A reassessment of
 490 prebiotic organic synthesis in neutral planetary atmospheres. *Orig. Life Evol. Biosph.* 38, 105–
 491 115. doi:10.1007/s11084-007-9120-3.
- 492 Corchado, J. C., Espinosa-Garcia, J., Hu, W.-P., Rossi, I., and Truhlar, D. G. (1995). Dual-Level
 493 Reaction-Path Dynamics (the /// Approach to VTST with Semiclassical Tunneling). Application
 494 to OH + NH₃ → H₂O + NH₂. *J. Phys. Chem.* 99, 687–694. doi:10.1021/j100002a037.
- 495 Diau, E. W. G., Tso, T. L., and Lee, Y. P. (1990). Kinetics of the reaction OH + NH₃ in the range
 496 273–433 K. *J. Phys. Chem.* 94, 5261–5265. doi:10.1021/j100376a018.
- 497 Ehrenfreund, P., Irvine, W., Becker, L., Blank, J., Brucato, J. R., Colangeli, L., et al. (2002).
 498 Astrophysical and astrochemical insights into the origin of life. *Reports Prog. Phys.* 65, 1427–

- 499 1487. doi:10.1088/0034-4885/65/10/202.
- 500 Espinosa-García, J., and Corchado, J. C. (1994). Analysis of certain factors in the direct dynamics
501 method: Variational rate constant of the $\text{NH}_3 + \text{OH} \rightarrow \text{NH}_2 + \text{H}_2\text{O}$ reaction. *J. Chem. Phys.* 101,
502 8700–8708. doi:10.1063/1.468065.
- 503 Förstel, M., Bergantini, A., Maksyutenko, P., Góbi, S., and Kaiser, R. I. (2017). Formation of
504 Methylamine and Ethylamine in Extraterrestrial Ices and Their Role as Fundamental Building
505 Blocks of Proteinogenic α -amino Acids. *Astrophys. J.* 845, 83. doi:10.3847/1538-4357/aa7edd.
- 506 Fourikis, N., Takagi, K., and Morimoto, M. (1974). Detection of Interstellar Methylamine by its
507 $2_{02} \rightarrow 1_{10}$ A_a-State Transition. *Astrophys. J.* 191, L139. doi:10.1086/181570.
- 508 Freeman, A., and Millar, T. J. (1983). Formation of complex molecules in TMC-1. *Nature* 301, 402–
509 404. doi:10.1038/301402a0.
- 510 Fujii, N., Chiba, K., Uchida, S., and Miyama, H. (1986). The rate constants of the elementary
511 reactions of NH_3 with O and OH. *Chem. Phys. Lett.* 127, 141–144. doi:10.1016/S0009-
512 2614(86)80243-3.
- 513 Fujii, N., Miyama, H., and Asaba, T. (1981). Determination of the rate constant for the reaction NH_3
514 $+ \text{OH} \rightarrow \text{NH}_2 + \text{H}_2\text{O}$. *Chem. Phys. Lett.* 80, 355–357. doi:10.1016/0009-2614(81)80125-X.
- 515 Galano, A., and Alvarez-Idaboy, J. R. (2008). Branching ratios of aliphatic amines + OH gas-phase
516 reactions: A variational transition-state theory study. *J. Chem. Theory Comput.* 4, 322–327.
517 doi:10.1021/ct7002786.
- 518 Garrod, R. T. (2013). A Three-phase Chemical Model of Hot Cores: The Formation of Glycine.
519 *Astrophys. J.* 765, 60. doi:10.1088/0004-637X/765/1/60.
- 520 Garrod, R. T., Weaver, S. L. W., and Herbst, E. (2008). Complex Chemistry in Star-forming
521 Regions: An Expanded Gas-Grain Warm-up Chemical Model. *Astrophys. J.* 682, 283–302.
522 doi:10.1086/588035.
- 523 Gerin, M., Neufeld, D. A., and Goicoechea, J. R. (2016). Interstellar Hydrides. *Annu. Rev. Astron.*
524 *Astrophys.* 54, 181–225. doi:10.1146/annurev-astro-081915-023409.
- 525 Gianturco, F. A., Yurtsever, E., Satta, M., and Wester, R. (2019). Modeling Ionic Reactions at
526 Interstellar Temperatures: The Case of $\text{NH}_2^+ + \text{H}_2 \rightleftharpoons \text{NH}_3 + \text{H}^+$. *J. Phys. Chem. A* 123, 9905–
527 9918. doi:10.1021/acs.jpca.9b07317.
- 528 Giménez, X., Moreno, M., and Lluch, J. M. (1992). Ab initio study of the $\text{NH}_3 + \text{OH}$ reaction. *Chem.*
529 *Phys.* 165, 41–46. doi:10.1016/0301-0104(92)80041-S.
- 530 Goicoechea, J. R., Joblin, C., Contursi, A., Berné, O., Cernicharo, J., Gerin, M., et al. (2011). OH
531 emission from warm and dense gas in the Orion Bar PDR. *Astron. Astrophys.* 530, L16.
532 doi:10.1051/0004-6361/201116977.
- 533 Hack, W., Hoyerman, K., and Wagner, H. G. (1974). Reaktionen des Hydroxylradikals mit
534 Ammoniak und Hydrazin in der Gasphase. *Ber. Bunsenges. Phys. Chem. Chem. Phys.* 78, 386–

- 535 391.
- 536 Halfen, D. T., Ilyushin, V. V., and Ziurys, L. M. (2013). Insights into surface hydrogenation in the
537 interstellar medium: observations of mathanimine and methyl amine Sgr B2(N). *Astrophys. J.*
538 767, 66. doi:10.1088/0004-637X/767/1/66.
- 539 Heard, D. E. (2018). Rapid Acceleration of Hydrogen Atom Abstraction Reactions of OH at Very
540 Low Temperatures through Weakly Bound Complexes and Tunneling. *Acc. Chem. Res.* 51,
541 2620–2627. doi:10.1021/acs.accounts.8b00304.
- 542 Herbst, E. (1985). The rate of the radiative association reaction between CH_3^+ and NH_3 and its
543 implications for interstellar chemistry. *Astrophys. J.* 292, 484–486. doi:10.1086/163179.
- 544 Herbst, E., and Klemperer, W. (1973). The Formation and Depletion of Molecules in Dense
545 Interstellar Clouds. *Astrophys. J.* 185, 505–533. doi:10.1086/152436.
- 546 Herbst, E., and van Dishoeck, E. F. (2009). Complex Organic Interstellar Molecules. *Annu. Rev.*
547 *Astron. Astrophys.* 47, 427–480. doi:10.1146/annurev-astro-082708-101654.
- 548 Hickson, K. M., Loison, J. C., Bourgalais, J., Capron, M., Picard, S. D. L., Goulay, F., et al. (2015).
549 The $\text{C}(^3\text{P}) + \text{NH}_3$ reaction in interstellar chemistry: II. Low temperature rate constants and
550 modeling of NH , NH_2 , and NH_3 abundances in dense interstellar clouds. *Astrophys. J.* 812, 1–
551 25. doi:10.1088/0004-637X/812/2/107.
- 552 Ioppolo, S., Fedoseev, G., Chuang, K. J., Cuppen, H. M., Clements, A. R., Jin, M., et al. (2021). A
553 non-energetic mechanism for glycine formation in the interstellar medium. *Nat. Astron.* 5, 197–
554 205. doi:10.1038/s41550-020-01249-0.
- 555 Jeffries, J. B., and Smith, G. P. (1986). Kinetics of the reaction $\text{OH} + \text{NH}_3$. *J. Phys. Chem.* 90, 487–
556 491. doi:10.1021/j100275a027.
- 557 Jiménez, E., Antiñolo, M., Ballesteros, B., Canosa, A., and Albaladejo, J. (2016). First evidence of
558 the dramatic enhancement of the reactivity of methyl formate ($\text{HC}(\text{O})\text{OCH}_3$) with OH at
559 temperatures of the interstellar medium: a gas-phase kinetic study between 22 K and 64 K.
560 *Phys. Chem. Chem. Phys.* 18, 2183–2191. doi:10.1039/C5CP06369H.
- 561 Jiménez, E., Ballesteros, B., Canosa, A., Townsend, T. M., Maigler, F. J., Napal, V., et al. (2015).
562 Development of a pulsed uniform supersonic gas expansion system based on an aerodynamic
563 chopper for gas phase reaction kinetic studies at ultra-low temperatures. *Rev. Sci. Instrum.* 86.
564 doi:10.1063/1.4918529.
- 565 Jiménez, E., Lanza, B., Garzón, A., Ballesteros, B., and Albaladejo, J. (2005). Atmospheric
566 degradation of 2-butanol, 2-methyl-2-butanol, and 2,3-dimethyl-2-butanol: OH kinetics and UV
567 absorption cross sections. *J. Phys. Chem. A* 109, 10903–10909. doi:10.1021/jp054094g.
- 568 Jonusas, M., Leroux, K., and Krim, L. (2020). N + H surface reaction under interstellar conditions:
569 Does the $\text{NH}/\text{NH}_2/\text{NH}_3$ distribution depend on N/H ratio? *J. Mol. Struct.* 1220, 128736.
570 doi:10.1016/j.molstruc.2020.128736.
- 571 Kaifu, N., Morimoto, M., Nagane, K., Akabane, K., Iguchi, T., and Takagi, K. (1974). Detection of

- 572 Interstellar Methylamine. *Astrophys. J.* 191, L135. doi:10.1086/181569.
- 573 Kim, Y. S., and Kaiser, R. I. (2011). On the formation of amines (RNH₂) and the cyanide anion (CN⁻)
574 in electron-irradiated ammonia-hydrocarbon interstellar model ices. *Astrophys. J.* 729.
575 doi:10.1088/0004-637X/729/1/68.
- 576 Kurylo, M. J. (1973). Kinetics of the reactions OH (v=0) + NH₃ → H₂O + NH₂ and OH(v=0) + O₃ →
577 HO₂ + O₂ at 298°K. *Chem. Phys. Lett.* 23, 467–471. doi:10.1016/0009-2614(73)89003-7.
- 578 Linnartz, H., Ioppolo, S., and Fedoseev, G. (2015). Atom addition reactions in interstellar ice
579 analogues. *Int. Rev. Phys. Chem.* 34, 205–237. doi:10.1080/0144235X.2015.1046679.
- 580 Lynch, B. J., Fast, P. L., Harris, M., and Truhlar, D. G. (2000). Adiabatic connection for kinetics. *J.*
581 *Phys. Chem. A* 104, 4813–4815. doi:10.1021/jp000497z.
- 582 Miller, S. L. (1953). A Production of Amino Acids Under Possible Primitive Earth Conditions.
583 *Science (80-)*. 117, 528–529. doi:10.1126/science.117.3046.528.
- 584 Monge-Palacios, M., Corchado, J. C., and Espinosa-Garcia, J. (2013a). Dynamics study of the OH +
585 NH₃ hydrogen abstraction reaction using QCT calculations based on an analytical potential
586 energy surface. *J. Chem. Phys.* 138, 1–12. doi:10.1063/1.4808109.
- 587 Monge-Palacios, M., and Espinosa-Garcia, J. (2013). Role of vibrational and translational energy in
588 the OH + NH₃ reaction: A quasi-classical trajectory study. *J. Phys. Chem. A* 117, 5042–5051.
589 doi:10.1021/jp403571y.
- 590 Monge-Palacios, M., Rangel, C., and Espinosa-Garcia, J. (2013b). Ab initio based potential energy
591 surface and kinetics study of the OH + NH₃ hydrogen abstraction reaction. *J. Chem. Phys.* 138,
592 084305. doi:10.1063/1.4792719.
- 593 Neeman, E. M., González, D., Blázquez, S., Ballesteros, B., Canosa, A., Antiñolo, M., et al. (2021).
594 The impact of water vapor on the OH reactivity toward CH₃CHO at ultra-low temperatures
595 (21.7–135.0 K): Experiments and theory. *J. Chem. Phys.* 155, 034306. doi:10.1063/5.0054859.
- 596 Nguyen, T. L., and Stanton, J. F. (2017). High-level theoretical study of the reaction between
597 hydroxyl and ammonia: Accurate rate constants from 200 to 2500 K. *J. Chem. Phys.* 147.
598 doi:10.1063/1.4986151.
- 599 Nielsen, C., D'Anna, B., Aursnes, M., and Boreave, A. (2012). Summary Report from Atmospheric
600 Chemistry Studies of Amines, Nitrosamines, Nitramines and Amides; Climit Project No.
601 208122. *NILU*, University of Oslo.
- 602 Nielsen, C. J., D'Anna, B., Karl, M., Aursnes, M., Boreave, A., Bossi, R., et al. (2011). Summary
603 Report: Photo-oxidation of Methylamine, Dimethylamine and Trimethylamine. Climit project
604 No. 201604. *NILU 2*, University of Oslo.
- 605 Nizamov, B., and Leone, S. R. (2004). Rate Coefficients and Kinetic Isotope Effect for the C₂H
606 Reactions with NH₃ and ND₃ in the 104–294 K Temperature Range. *J. Phys. Chem. A* 108,
607 3766–3771. doi:10.1021/jp031361e.

- 608 Nyman, G. (1996). Quantum scattering calculations on the $\text{NH}_3+\text{OH}\rightarrow\text{NH}_2+\text{H}_2\text{O}$ reaction. *J. Chem.*
609 *Phys.* 104, 6154–6167. doi:10.1063/1.471281.
- 610 Ocaña, A. J., Blázquez, S., Ballesteros, B., Canosa, A., Antiñolo, M., Albaladejo, J., et al. (2018).
611 Gas phase kinetics of the $\text{OH} + \text{CH}_3\text{CH}_2\text{OH}$ reaction at temperatures of the interstellar medium
612 ($T=21\text{--}107\text{K}$). *Phys. Chem. Chem. Phys.* 20, 5865–5873. doi:10.1039/C7CP07868D.
- 613 Ocaña, A. J., Blázquez, S., Potapov, A., Ballesteros, B., Canosa, A., Antiñolo, M., et al. (2019). Gas-
614 phase reactivity of CH_3OH toward OH at interstellar temperatures (11.7-177.5 K): Experimental
615 and theoretical study. *Phys. Chem. Chem. Phys.* 21, 6942–6957. doi:10.1039/c9cp00439d.
- 616 Ocaña, A. J., Jiménez, E., Ballesteros, B., Canosa, A., Antiñolo, M., Albaladejo, J., et al. (2017). Is
617 the Gas-phase $\text{OH}+\text{H}_2\text{CO}$ Reaction a Source of HCO in Interstellar Cold Dark Clouds? A
618 Kinetic, Dynamic, and Modeling Study. *Astrophys. J.* 850, 28. doi:10.3847/1538-4357/aa93d9.
- 619 Ohishi, M., Suzuki, T., Hirota, T., Saito, M., and Kaifu, N. (2019). Detection of a new methylamine
620 (CH_3NH_2) source: Candidate for future glycine surveys. *Publ. Astron. Soc. Japan* 71, 1–11.
621 doi:10.1093/pasj/psz068.
- 622 Onel, L., Blitz, M., Dryden, M., Thonger, L., and Seakins, P. (2014). Branching ratios in reactions of
623 OH radicals with methylamine, dimethylamine, and ethylamine. *Environ. Sci. Technol.* 48,
624 9935–9942. doi:10.1021/es502398r.
- 625 Onel, L., Thonger, L., Blitz, M. A., Seakins, P. W., Bunkan, A. J. C., Solimannejad, M., et al. (2013).
626 Gas-phase reactions of OH with methyl amines in the presence or absence of molecular oxygen.
627 an experimental and theoretical study. *J. Phys. Chem. A* 117, 10736–10745.
628 doi:10.1021/jp406522z.
- 629 Perry, R. A., Atkinson, R., and Pitts Jr, j. N. (1976). Rate constants for the reactions
630 $\text{OH}+\text{H}_2\text{S}\rightarrow\text{H}_2\text{O}+\text{SH}$ and $\text{OH}+\text{NH}_3\rightarrow\text{H}_2\text{O}+\text{NH}_2$ over the temperature range 297–427 °K. *J.*
631 *Chem. Phys.* 64, 3237. doi:10.1063/1.432663.
- 632 Potapov, A., Canosa, A., Jiménez, E., and Rowe, B. (2017). Uniform Supersonic Chemical Reactors:
633 30 Years of Astrochemical History and Future Challenges. *Angew. Chemie Int. Ed.* 56, 8618–
634 8640. doi:10.1002/anie.201611240.
- 635 Rednyk, S., Roučka, Kovalenko, A., Tran, T. D., Dohnal, P., Plašil, R., et al. (2019). Reaction of
636 NH^+ , NH_2^+ , and NH_3^+ ions with H_2 at low temperatures. *Astron. Astrophys.* 625, 1–8.
637 doi:10.1051/0004-6361/201834149.
- 638 Salimian, S., Hanson, R. K., and Kruger, C. H. (1984). High temperature study of the reactions of O
639 and OH with NH_3 . *Int. J. Chem. Kinet.* 16, 725–739. doi:10.1002/kin.550160609.
- 640 Sandford, S. A., Nuevo, M., Bera, P. P., and Lee, T. J. (2020). Prebiotic Astrochemistry and the
641 Formation of Molecules of Astrobiological Interest in Interstellar Clouds and Protostellar Disks.
642 *Chem. Rev.* 120, 4616–4659. doi:10.1021/acs.chemrev.9b00560.
- 643 Scott, G. B. I., Freeman, C. G., and McEwan, M. J. (1997). The interstellar synthesis of ammonia.
644 *Mon. Not. R. Astron. Soc.* 290, 636–638. doi:10.1093/mnras/290.4.636.

- 645 Silver, J. A., and Kolb, C. E. (1980). Rate constant for the reaction $\text{NH}_3 + \text{OH} \rightarrow \text{NH}_2 + \text{H}_2\text{O}$ over a
646 wide temperature range. *Chem. Phys. Lett.* 75, 191–195. doi:10.1016/0009-2614(80)80492-1.
- 647 Sims, I. R., Queffelec, J. L., Defrance, A., RebrionRowe, C., Travers, D., Bocherel, P., et al. (1994).
648 Ultralow temperature kinetics of neutral – neutral reactions . The technique and results for the
649 reactions $\text{CN} + \text{O}_2$ down to 13 K and $\text{CN} + \text{NH}_3$ down to 25 K. *J. Chem. Phys.* 100, 4229–4241.
650 doi:10.1063/1.467227.
- 651 Sleiman, C., El Dib, G., Rosi, M., Skouteris, D., Balucani, N., and Canosa, A. (2018a). Low
652 temperature kinetics and theoretical studies of the reaction $\text{CN} + \text{CH}_3\text{NH}_2$: A potential source of
653 cyanamide and methyl cyanamide in the interstellar medium. *Phys. Chem. Chem. Phys.* 20,
654 5478–5489. doi:10.1039/c7cp05746f.
- 655 Sleiman, C., El Dib, G., Talbi, D., and Canosa, A. (2018b). Gas Phase Reactivity of the CN Radical
656 with Methyl Amines at Low Temperatures (23-297 K): A Combined Experimental and
657 Theoretical Investigation. *ACS Earth Sp. Chem.* 2, 1047–1057.
658 doi:10.1021/acsearthspacechem.8b00098.
- 659 Smith, I. W. M., and Barnes, P. W. (2013). Advances in low temperature gas-phase kinetics. *Annu.*
660 *Reports Prog. Chem. - Sect. C* 109, 140–166. doi:10.1039/c3pc90011h.
- 661 Sorrell, W. H. (2001). Origin of Amino Acids and Organic Sugars in Interstellar Clouds. *Astrophys.*
662 *J.* 555, L129–L132. doi:10.1086/322525.
- 663 Stephens, R. D. (1984). Absolute rate constants for the reaction of hydroxyl radicals with ammonia
664 from 297 to 364 K. *J. Phys. Chem.* 88, 3308–3313. doi:10.1021/j150659a034.
- 665 Stuhl, F. (1973). Absolute rate constant for the reaction $\text{OH} + \text{NH}_3 \rightarrow \text{NH}_2 + \text{H}_2\text{O}$. *J. Chem. Phys.* 59,
666 635–637. doi:10.1063/1.1680069.
- 667 Taylor, S. E., Goddard, A., Blitz, M. A., Cleary, P. A., and Heard, D. E. (2008). Pulsed Laval nozzle
668 study of the kinetics of OH with unsaturated hydrocarbons at very low temperatures. *Phys.*
669 *Chem. Chem. Phys.* 10, 422–437. doi:10.1039/B711411G.
- 670 Theule, P., Borget, F., Mispelaer, F., Danger, G., Duvernay, F., Guillemin, J. C., et al. (2011).
671 Hydrogenation of solid hydrogen cyanide HCN and methanimine CH_2NH at low temperature.
672 *Astron. Astrophys.* 534, A64. doi:10.1051/0004-6361/201117494.
- 673 Tian, W., Wang, W., Zhang, Y., and Wang, W. (2009). Direct dynamics study on the mechanism and
674 the kinetics of the reaction of CH_3NH_2 with OH. *Int. J. Quantum Chem.* 109, 1566–1575.
675 doi:10.1002/qua.22000.
- 676 Vahedpour, M., Douroudgari, H., Afshar, S., and Asgharzade, S. (2018). Comparison of atmospheric
677 reactions of NH_3 and NH_2 with hydroxyl radical on the singlet, doublet and triplet potential
678 energy surfaces, kinetic and mechanistic study. *Chem. Phys.* 507, 51–69.
679 doi:10.1016/j.chemphys.2018.03.022.
- 680 van Dishoeck, E. F., Jansen, D. J., Schilke, P., and Phillips, T. G. (1993). Detection of the Interstellar
681 NH_2 Radical. *Astrophys. J.* 416, L83. doi:10.1086/187076.

- 682 Weinreb, S., Barret, A. H., Meeks, M. L., and Henry, J. C. (1963). Radio Observations of OH in the
683 Interstellar Medium. *Nature* 200, 829–831. doi:10.1038/200829a0.
- 684 Wilson, T. L., Gaume, R. A., and Johnston, K. J. (1993). Ammonia in the W3(OH) region.
685 *Astrophys. J.* 402, 230. doi:10.1086/172126.
- 686 Woon, D. E. (2002). Pathways to Glycine and Other Amino Acids in Ultraviolet-irradiated
687 Astrophysical Ices Determined via Quantum Chemical Modeling. *Astrophys. J.* 571, L177–
688 L180. doi:10.1086/341227.
- 689 Woon, D. E. (2021). A continuously updated list of the observed molecules is available online:
690 <http://www.astrochymist.org>.
- 691 Zabielski, M. F., and Seery, D. J. (1985). High temperature measurements of the rate of the reaction
692 of OH with NH₃. *Int. J. Chem. Kinet.* 17, 1191–1199. doi:10.1002/kin.550171105.
- 693 Zellner, R., and Smith, I. W. M. (1974). Rate constants for the reactions of OH with NH₃ and HNO₃.
694 *Chem. Phys. Lett.* 26, 72–74. doi:10.1016/0009-2614(74)89086-X.

695

696 **Tables**

697

698 **Table 1.** Summary of the experimental conditions (total gas density (n), jet pressure (p), and reactant
699 concentration in the jet) and corrected *pseudo*-first order rate coefficient ranges.

Reactant	Laval nozzle	$n / 10^{16} \text{ cm}^{-3}$	p / mbar	$[\text{Reactant}] / 10^{13} \text{ cm}^{-3}$	$k' - k_0' / \text{s}^{-1}$	$k(T) / 10^{-11} \text{ cm}^3 \text{ s}^{-1}$
NH ₃	He23-HP	16.7	0.51	4.2 – 21.6	1932 – 5613	2.7 ± 0.1
	He23-IP	7.4	0.23	3.5 – 10.7	1177 – 2737	2.7 ± 0.1
	He23-LP	3.4	0.10	2.9 – 8.6	408 – 2886	2.9 ± 0.3
CH ₃ NH ₂	He23-HP	16.7	0.51	0.3 – 3.1	589 – 11713	39.2 ± 2.0
	He23-IP	7.4	0.23	0.7 – 3.1	3317 – 11166	36.2 ± 1.4
	He23-LP	3.4	0.10	0.6 – 2.9	2382 – 12034	41.1 ± 1.5

700

701

702

703
704
705
706
707
708**Table 2.** Summary of the calculated energies relative to reactants (in kcal/mol) of the stationary points in the MEP for the OH+NH₃ reaction reported in the literature (see text for more details).

PRC	TS	PPC	Products	References
	8.94		-10.69 ^(a)	(Giménez et al., 1992)
	9.05	-15.02	-8.98	Espinosa-García and Corchado (1994)
-1.75	3.65	-17.39	-11.96	Corchado et al. (1995)
	2.03			Bowdridge et al. (1996)
	4.4		-7.1	Lynch et al. (2000)
-1.8	3.3	-15.6	-10.0	Monge-Palacios et al. (2013b)
0.33	2.6	-14.47	-11.49	Nguyen and Stanton (2017)

709

^(a) From $\Delta H_r^0_{298\text{ K}}$

710

Table 3. Summary of the calculated relative (to reactants) energies (in kcal/mol) of the stationary points in the MEP for the OH+CH₃NH₂ reaction reported in the literature (see text for more details).711
712

Channel	PRC	TS	PPC	Products	References
R2a		0.36		-23.19	Galano and Alvarez-Idaboy (2008)
R2b		0.97		-17.00	
R2a	-0.61	-0.52	-28.48	-23.17	Tian et al. (2009)
R2b	-8.45	1.02	-23.03	-17.07	
R2a	-6.38	-1.96	-29.54	-43.52	Onel et al. (2013)
R2b	-6.38	-2.0	-24.19	-26.48	
R2a	-5.4	1.2		-26.0	Borduas et al. (2016)
R2b	-0.2	0.2		-19.0	

713

714

715 **Figure legends**

716 **Scheme 1.** Simplified reaction energy profile along the MEP for the OH + NH₃ reaction.

717

718 **Scheme 2.** Simplified reaction energy profile along the MEP for the OH + CH₃NH₂ reaction.

719

720 **Fig 1.** Examples of the I_{LIF} temporal profile in the presence of similar concentrations of NH₃ (a) and
721 CH₃NH₂ (b) for a total gas density of $7.4 \times 10^{16} \text{ cm}^{-3}$.

722

723 **Fig. 2.** Example of the observed curvature in the bimolecular plots for the OH + CH₃NH₂ reaction at
724 ca. 22 K and $3.4 \times 10^{16} \text{ cm}^{-3}$. Solid line represents k_2 obtained from the fit of all data from Fig. 3.

725

726 **Fig. 3.** Bimolecular plots for the OH-reactions at ca. 22 K with (a) NH₃ and (b) CH₃NH₂.

727

728 **Fig. 4.** (a) Temperature dependence of k_1 (log-log plot) in the 22-4000 K range. Individual rate
729 coefficients at room temperature K (Zellner and Smith, 1974; Perry et al., 1976; Silver and Kolb,
730 1980; Stephens, 1984; Diau et al., 1990) are not included in the figure, but they are considered in the
731 IUPAC recommendation (red curve). (b) Arrhenius plot for k_1 between 170 K and 4000 K to better
732 see the curvature (non-Arrhenius behavior). (c) Extension of the log-log plot shown in (a) to show
733 the great enhancement of k_1 with respect to theoretical predictions at 20 K.

734

735 **Fig. 5.** Temperature dependence of k_2 in the 22-3000 K range.

736

737